

Article

Asymmetric Constrained Control of a Cervical Orthotic Device Based on Barrier Sliding Modes

Caridad Mireles ^{1,2}, Alejandro Lozano ^{2,†}, Mariana Ballesteros ^{1,2}, David Cruz-Ortiz ² and Ivan Salgado ^{1,*}

¹ Centro de Innovación y Desarrollo Tecnológico en Cómputo, Instituto Politécnico Nacional, Mexico City 07700, Mexico

² Medical Robotics and Biosignal Processing Laboratory, Unidad Profesional Interdisciplinaria de Biotecnología, Instituto Politécnico Nacional, Mexico City 07340, Mexico

* Correspondence: isalgador@ipn.mx

† Current address: Department of Biomedical Data Science, Stanford University, Stanford, CA 94305, USA.

Abstract: This work proposes a robust sliding mode controller to enforce the tracking trajectory of a cervical orthotic device subjected to asymmetric box constraints. The convergence analysis employs an asymmetric barrier Lyapunov function (ABLF), whose argument is a restricted sliding surface. The stability analysis demonstrates the finite-time convergence of the states towards the sliding surface and, therefore, the exponential stability of the system trajectories. The controller ensures the fulfillment of the restrictions imposed on the sliding surface and consequently over the states. Numerical simulations exhibit the performance of the proposed controller ensuring restricted movements for flexion and extension of a virtual orthotic cervical device. The restricted movements obey asymmetric constraints according to the therapies proposed by medical specialists.

Keywords: asymmetric box-type constraints; barrier Lyapunov function; first-order sliding modes; finite-time convergence



Citation: Mireles, C.; Lozano, A.; Ballesteros, M.; Cruz-Ortiz, D.; Salgado, I. Asymmetric Constrained Control of a Cervical Orthotic Device Based on Barrier Sliding Modes. *Appl. Sci.* **2022**, *12*, 10286. <https://doi.org/10.3390/app122010286>

Academic Editor: Jesús Picó

Received: 27 August 2022

Accepted: 4 October 2022

Published: 13 October 2022

Publisher's Note: MDPI stays neutral with regard to jurisdictional claims in published maps and institutional affiliations.



Copyright: © 2022 by the authors. Licensee MDPI, Basel, Switzerland. This article is an open access article distributed under the terms and conditions of the Creative Commons Attribution (CC BY) license (<https://creativecommons.org/licenses/by/4.0/>).

1. Introduction

1.1. Preliminaries

Currently, emerging technologies provide feasible solutions for medical problems [1]. In terms of physical medicine and rehabilitation, the improvement of classical static orthosis and prosthesis has helped patients to recover their functional abilities in a shorter period of time [2]. Static orthosis usually immobilizes or restricts the motion of human limbs. They are made with diverse materials depending on their applications [3]. On the other hand, an active orthosis is a device that increases the ability of a person suffering from pathology or a fracture augmenting the power at one or more joints of the extremities by means of a mechanical actuated structure [4]. Depending on the physical affectation, the specialists should suggest the kind of orthosis to use. Cervical orthoses are a particular case of these devices which are designed to control head movement and neck function, cervical orthoses vary greatly in the degree to which they immobilize the neck and unload head weight [5,6].

The most common cervical orthoses applications include the physiotherapy of head pain such as migraines [7], correction of spinal deformities, rehabilitation in postoperative procedures [8], whiplash-associated disorders, and non-operative treatment for fractures [9,10]. Some examples are the halo vest, Philadelphia collars, Minerva collars, aspen, stiff-neck Miami collar, among others [3,11]. Even though, several studies support the effectiveness of these orthoses immobilizing the fracture sites [10], current studies have demonstrated the advantages of using active orthoses, not only in cervical injuries but also in lower-limb rehabilitation [12]. The design of a cervical orthosis must satisfy the support, prevention, and correction of cervical injuries in patients [3]. Moreover, it must satisfy three-point pressure in parts of the body where nerves and tissues are not affected by the structure system [13]; the manufacturing of cervical orthosis devices should

be circumferential for supporting the neck and limiting the range of motion. In addition, the manufacturing device needs to be elaborated with material that does not irritate the skin. Indeed, some researchers evaluated different types of orthosis that have effects on the quality of treatment depending if the injury is a fracture, postoperative treatment, or deformity [14]. The main parameters to be evaluated in the design of an orthosis are the restricted motion, the correct size, comfort assessment control of snaking, and control of flexion/extension/rotation [8,10]. Some evaluations compare the efficiency of common cervical orthosis finding the main complications of wearing those devices [10]. The main issues related to wearing a cervical orthosis are infections, pressure in plastic vests, injuries in nerves, occipital ulceration, stiffness of facial muscles, and control motion [8,15].

Robotic cervical orthoses have to ensure a correct control range of motion during rehabilitation for either postoperative surgeries, fractures, or cervical injuries during rehabilitation sessions [16,17]. Some of them use new mechanical technologies for their design, as well as control algorithms to ensure the safety and correct treatment of the patient. The robotic cervical systems which are bio-inspired designs usually incorporate the measurements of bio-potentials such as electromyography or electroencephalography for active control [17–20].

Therefore, the control theory applied in any orthosis device must guarantee the security of the patient during the tracking trajectory of natural neck motion [17]. Among others, adaptive controllers, impedance adaptive controllers [21], and active disturbance theory [22] have been used in the control of active orthoses. To enhance the safety capacity of active cervical orthoses, the control development ought to consider movement and velocity restrictions. Barrier Lyapunov functions (BLF) have been implemented to deal with state and control restrictions [23]. BLFs have solved many problems related to state restrictions. The main idea of this strategy is to produce a strong control signal when the system trajectories approach a given boundary [24]. The strategies developed under the concept of BLFs include robust controllers using a constrained attractive ellipsoid approach [25], adaptive constrained control [26,27], neuroadaptive learning algorithm for constrained nonlinear systems based on time-varying barrier Lyapunov functions [28], sliding mode control [23], among others.

Sliding mode control offers attractive features such as robustness against matched perturbations, finite-time convergence, and model reduction [23,29]. For mechanical systems, this theory is mainly selected when the system is partially unknown. Restricted sliding modes (SM) ensure the accomplishment of position and velocities through the restriction of the sliding motion. To reach this goal, logarithmic BLFs have been implemented in first-order sliding modes (FOSM) and terminal SM. However, it considers only symmetric restrictions that do not fulfill the requirements for an active orthosis, where the movement is restricted according to the injury or the natural movement of the human limbs.

The work in [30] develops a robotic neck controlled with a proportional–integral–derivative (PID) control strategy to coordinate head movement in patients with different neurological disorders, such as amyotrophic lateral sclerosis and cerebral palsy. For whiplash syndrome, the authors of [21] provide an impedance adaptive PID controlled device for rehabilitation. Notice that these two approaches do not consider state restrictions that can damage the patient if an overshoot appears in the control signal. The authors of [31] propose a novel mechanical design for a neck orthosis implementing a restricted non-terminal sliding mode with a convergence proof based on a logarithmic BLF. The controller ensures the fulfillment of symmetric box-type constraints.

1.2. Contributions

The work presented in [26] deals with the design of an adaptive asymptotic tracking control for a class of uncertain nonlinear systems with parametric uncertainties. An asymmetric BLF (ABLF) achieves asymptotic convergence with zero-tracking error, bounded closed-loop signals, and the fulfillment of asymmetric state restrictions. This manuscript introduces an ABLF for SM controllers. The main contributions of this work includes the

design of an asymmetric controller based on first order sliding modes and a BLF, and its implementation for controlling a virtual robotic orthosis.

1.3. Manuscript Organization

The organization of the manuscript is the following: Section 2 introduces some mathematical definitions to understand the control design. Section 3 defines the problem statement with the requirements the controller have to consider dealing with a robotic orthosis. Section 4 describes the mathematical representation for a mechanical orthosis device that obeys a fully actuated second-order nonlinear system. The nature of the constraints are addressed in this section. Section 5 purposes an asymmetric FOSM control strategy for second-order systems with asymmetric state restrictions. This section summarizes the main result in the main theorem. In Section 6, some numerical simulations show the behavior of the proposed controller. Some comparisons against classical strategies demonstrate the advantages of using the constrained first-order sliding mode controller. Finally, some remarks are given in Section 7.

2. Mathematical Preliminaries

The solution of the problem proposed in this manuscript requires some well-known mathematical preliminaries.

Definition 1. (*Barrier Lyapunov function [32]*). Let $\Omega \subset \mathbb{R}^n$ represents an open set with the boundary $\partial\Omega$, and $V : \Omega \rightarrow \mathbb{R}^+$ be a continuous function in \mathbb{R}^+ , it means V is a BLF if it is positive definite, continuously differentiable in Ω , as

$$\limsup_{x \rightarrow \partial\Omega^-} V(x(t)) \rightarrow +\infty,$$

and $V(x(t)) \leq b, \forall t \geq 0$ for some $b \in \mathbb{R}^+$ and for any $x(0) \in \Omega$. If $\dot{V}(x(t)) \leq 0$ and $x(0) \in \Omega$ then, $b = V(x(0))$ and any future trajectory is bounded in Ω .

Lemma 1. For any constant $|\rho| < 1$, the following inequalities are satisfied

$$\begin{aligned} a) \quad & \rho \leq -\log(1 - \rho) \leq \frac{\rho}{1 - \rho} \\ b) \quad & -\frac{\rho^2}{1 - \rho^2} \leq -\log\left(\frac{1}{1 - \rho^2}\right) \end{aligned}$$

Proof. The proof of this Lemma is analyzed in [23]. \square

Lemma 2 ([23]). Let ρ a positive constant satisfying $|\rho| \leq 1$, then, the following inequality holds

$$-\frac{1}{\rho} \leq -\frac{1}{\log \sqrt{\frac{1}{1 - \rho^2}}} \quad (1)$$

3. Problem Statement

Physical real systems should consider state restrictions that can be maximum and minimum values for both, position and velocity. In the case of robotic systems used in medical applications (like robotic orthosis and prosthesis). These restrictions play an important role designing control strategies to avoid any damage or undesired movement that can affect the patient. For the cervical orthosis designed in this manuscript, as a consequence of a particular muscle injury, some positions can not be attainable by the patient. Therefore, a cervical orthotic device should consider asymmetric restrictions in position and velocity. The problem to solve can be summarized as follows:

The control problem in this manuscript aims to design an effective robust tracking control for the orthosis mechanical system such that a) the origin becomes an asymptotic equilibrium point for the tracking error; b) all signals in closed-loop systems are bounded; and c) the full asymmetric state constraints are not violated.

To deal with this problem statement, the following mathematical tools will be applied developing the stability proof of the proposed controller.

4. Mathematical Description of the Cervical Orthotic Device

The mathematical description consider to be fulfilled by the mechanical orthosis device is obtained through the Euler–Lagrange approach. Therefore, the following mathematical model can describe the complete dynamics of the orthosis [23]

$$\ddot{q}(t) = F(\dot{q}(t), t) + G(q(t), t) + \Psi(q(t), t), \tag{2}$$

with $q(0) = q_0$ and $\dot{q}(0) = \dot{q}_{d0}$ being the initial conditions, $q_0, \dot{q}_{d0} \in \mathbb{R}^n$. $q \in \mathbb{R}^{2n}$ is the vector of generalized coordinates and $\dot{q} \in \mathbb{R}^{2n}$ its corresponding derivative. Function $F : \mathbb{R}^{2n} \times \mathbb{R}^+ \rightarrow \mathbb{R}^n$ is the drift term and it satisfies the Lipchitz condition and the term $G : \mathbb{R}^n \times \mathbb{R}^+ \rightarrow \mathbb{R}^{n \times n}$ is a known matrix associated with the input signal $u \in \mathbb{R}^n$. The nonlinear function $\Psi : \mathbb{R}^{2n} \times \mathbb{R}^+ \rightarrow \mathbb{R}^n$ represents uncertainties and non-modeling dynamics that satisfies the next condition

$$\|\Psi(q, t)\| \leq \Psi_0 + \Psi_1 \|q\|^2, \quad \Psi_0, \Psi_1 \in \mathbb{R}^+. \tag{3}$$

defining $x_1 = q$ and $x_2 = \dot{q}$, by the state variable approach, system in (2) becomes (the time dependence is omitted to facilitate the reading of the manuscript)

$$\begin{aligned} \dot{x}_1 &= x_2 \\ \dot{x}_2 &= f(x, t) + g(x_1)u + \Psi(x, t), \end{aligned} \tag{4}$$

where $x_1 = [x_{1,1} \ x_{1,2} \ \dots \ x_{1,n}]^\top$ and $x_2 = [x_{2,1} \ x_{2,2} \ \dots \ x_{2,n}]^\top$.

As it was mentioned before, the orthotic device should be restricted in movement and velocity. Therefore, the following assumption is taking into account in this manuscript.

Assumption 1. *The states are bounded by*

$$x_1^- \leq \|x_1(t)\|^2 \leq x_1^+, \quad x_2^- \leq \|x_2(t)\|^2 \leq x_2^+, \quad \forall t \geq 0,$$

with $x_{1,+}$, $x_{2,+}$ being positive known constants and $x_{2,-}$ and $x_{1,-}$ being negative constants. For n -dimensional systems, it is possible to assume that each state is bounded individually by

$$\begin{aligned} k_{c_{1,i}}^- \leq x_{1,i} \leq k_{c_{1,i}}^+, & \quad k_{c_{2,i}}^- \leq x_{2,i} \leq k_{c_{2,i}}^+ \\ k_{c_{1,i}}^+, k_{c_{2,i}}^+ \in \mathbb{R}^+, & \quad k_{c_{1,i}}^-, k_{c_{2,i}}^- \in \mathbb{R}^-, \end{aligned}$$

previous equation implies an asymmetric box-type constraints for the second order system in (2).

Remark 1. *The definition of the constraints in Assumption 1, without loss of generality, implies asymmetric-type box constraints centered at zero. For positive asymmetric constraints, a transformation can be implemented to apply the control design proposed in this manuscript.*

Assumption 2. *The nonlinear function $f(x, t)$ accepts the next upperbound*

$$\|f(t, x)\|^2 \leq f_0 + f_1 \|x\|^2, \quad f_0, f_1 \in \mathbb{R}^+,$$

based on Assumption 1, previous inequality is equivalent to

$$f^- \leq \|f(t, x)\|^2 \leq f^+,$$

where $f^- = f_0 + f_1x^-$ and $f^+ = f_0 + f_1x^+$

As a consequence of the restrictions imposed over the physical system, the tracking trajectories should be restricted according the next assumption.

Assumption 3. The vector of target signals y_r and its first time derivative \dot{y}_r are continuous and bounded. Moreover, the i th components of y_r and \dot{y}_r called $y_{r,i}$ and $\dot{y}_{r,i}$, respectively, accepts the following bounds

$$\begin{aligned} k_{c_{1,i}}^- \leq y_{r,i}^- \leq y_{r,i} \leq y_{r,i}^+ \leq k_{c_{1,i}}^+ \\ k_{c_{2,i}}^- \leq dy_{r,i}^- \leq \dot{y}_{r,i} \leq dy_{r,i}^+ \leq k_{c_{2,i}}^+ \end{aligned}$$

Based on Assumptions 1 and 3, the tracking error defined as $z = x - \bar{y}_r$ should be bounded inside an asymmetric box-type constraints. Here $\bar{y}_r := [y_r^\top \dot{y}_r^\top]^\top$ and $x := [x_1^\top x_2^\top]^\top$. The associated restrictions are given by

$$k_{a_i} \leq z_{1,i} \leq k_{b_i} \quad dk_{a_i} \leq z_{2,i} \leq dk_{b_i}, \tag{5}$$

where $k_{b_i} = k_{c_{1,i}}^+ - y_{r,i}^-$, $dk_{a_i} = k_{c_{1,i}}^- - y_{r,i}^+$, $dk_{b_i} = k_{c_{2,i}}^+ - dy_{r,i}^-$, and $dk_{a_i} = k_{c_{2,i}}^- - dy_{r,i}^+$.

5. Control Design Based on an Asymmetric Barrier Lyapunov Function

The control strategy adopts the well-known FOSM theory. SM theory implies the selection of a sliding surface with a desirable convergence behavior and a control algorithm to enforce the reaching of the surface in finite time. An ABLF analyzes the equilibrium point of the tracking error.

System Decomposition

The uncertain system (4) can be decomposed as n -second order systems, that is,

$$\begin{aligned} \dot{x}_{1,i} &= x_{2,i} \\ \dot{x}_{2,i} &= f_i(x) + g_i(x_{1,i})u_i + \sum_{j=1, j \neq i}^n g_{i,j}(x_1)u_j + \psi_i(x_1, t), \end{aligned} \tag{6}$$

where g_i is the diagonal matrix taking the element $g_{i,i}$ of matrix $G(x)$ i -th element of function, f_i is the i th element of function F . The matrix $g_{i,j}$ groups the effect of the remaining control actions u_j with $i \neq j$. Taking into account the definition of the tracking error z_i , its dynamics becomes

$$\begin{aligned} \dot{z}_{1,i} &= z_{2,i} \\ \dot{z}_{2,i} &= f_i(x) + g_i(x_{1,i})u_i + \sum_{j=1, j \neq i}^n g_{i,j}(x_1)u_j + \psi_i(x_1, t) - \dot{y}_{r,i}. \end{aligned} \tag{7}$$

Let proposes the following control to solve the tracking trajectory task

$$u_i = g_i^{-1}(u_{a,i} + u_{b,i}), \tag{8}$$

in last equation, the component $u_{a,i}$ compensates the nonlinear dynamics and the interaction of the control components in the i -th state, that is

$$u_{a_i} = \begin{cases} -f^+ - \gamma_i z_{2,i} - \sum_{i=1, i \neq j}^n g_{i,j} u_{i,j} + \ddot{y}_{r,i} & \text{if } \sigma(s_i) = 1 \\ -f^- - \gamma_i z_{2,i} - \sum_{i=1, i \neq j}^n g_{i,j} u_{i,j} + \ddot{y}_{r,i} & \text{if } \sigma(s_i) = 0 \end{cases} \tag{9}$$

the definition of function $\sigma(\cdot)$ is

$$\sigma(\cdot) := \begin{cases} 1 & \text{if } \cdot > 0 \\ 0 & \text{if } \cdot \leq 0 \end{cases} \tag{10}$$

and s_i is the i -th component of the sliding surface, which is defined as,

$$s_i = z_{2,i} + \gamma_i z_{1,i}, \tag{11}$$

here, $\gamma_i \in \mathbb{R}^+$ defines the rate of convergence of the tracking error. The control component u_{b_i} forces the tracking error to converge in finite time to the sliding surface defined in (11), and it has the following definition

$$u_{b_i} = -\bar{k}_i(t) \text{sign}(s_i) \\ \bar{k}_i := \begin{cases} \tilde{k}_i^+ & \text{if } \sigma(s_i) = 1 \\ \tilde{k}_i^- & \text{if } \sigma(s_i) = 0 \end{cases} \tag{12}$$

the definition of the adaptive gains are the following

$$\tilde{k}_i^+ = \bar{k}_{s_i} (0.5)^{\frac{3}{2}} \mu_i \frac{1}{1 - \eta_{b,i}} + \text{sign}(\eta_{b_i}) \frac{\Psi_i^+}{1 - \eta_{b,i}}, \\ \tilde{k}_i^- = \underline{k}_{s_i} (0.5)^{\frac{3}{2}} \mu_i \frac{1}{1 - \eta_{a,i}} + \text{sign}(\eta_{a_i}) \frac{\Psi_i^-}{1 - \eta_{a,i}}, \tag{13}$$

with $\mu_i \geq 0$. The values of $\eta_{a,i}$ and $\eta_{b,i}$ are defined as

$$\eta_{a_i} := \frac{s_i}{\underline{k}_{s_i}}, \quad \eta_{b_i} := \frac{s_i}{\bar{k}_{s_i}}, \tag{14}$$

and s_i is the sliding surface, that is,

$$s_i = z_{2,i} + \gamma_i z_{1,i}. \tag{15}$$

Notice that the sliding surface has the following bounds based on the constraints imposed over the states

$$\underline{k}_{s_i} \leq s_i(t) \leq \bar{k}_{s_i}, \quad \forall t \geq 0 \\ \underline{k}_{s_i} := dk_{a_i} + \gamma_i k_{a_i}, \quad \bar{k}_{s_i} := dk_{b_i} + \gamma_i k_{b_i}. \tag{16}$$

The main result of this manuscript is given in the following Theorem

Theorem 1. *Let consider the close-loop system in (7) that represents the tracking error for a mechanical system in form of Equation (6). If the control action is selected as in Equation (8) with*

$\mu > 0$ and the time varying gains described by Equation (13). Then, the origin of the sliding surface is a finite-time equilibrium point with a convergence time defined as

$$T(s) \leq \sqrt[4]{0.5} \min_{i \in \{1, 2, \dots, n\}} \left(\frac{\sqrt{V(s_i)}}{\mu_i^{0.5}} \right), \tag{17}$$

and the tracking error has an asymptotically stable equilibrium point at the origin.

Proof. Consider the following ABLF

$$V(s(t)) := \sum_{i=1}^n V_i(s_i(t)),$$

where the i -th element is

$$V_i = \frac{\sigma(s_i)}{2} \log \left(\frac{\bar{k}_{s_i}^2}{\bar{k}_{s_i}^2 - s_i^2} \right) + \frac{1 - \sigma(s_i)}{2} \log \left(\frac{k_{s_i}^2}{k_{s_i}^2 - s_i^2} \right). \tag{18}$$

These function takes into account the approaches developed in [23,26]. With the function σ defined in Equation (10). Defining the variable η_i as

$$\eta_i := \sigma(s_i)\eta_{b_i} + (1 - \sigma(s_i))\eta_{a_i}, \tag{19}$$

equation in (18) becomes

$$V_i := \frac{1}{2} \log \frac{1}{1 - \eta_i^2}, \tag{20}$$

notice that $\eta_i > 0$ for any time great or equal to zero. Therefore, V_1 is a positive definite and continuously differentiable function. Its first time derivative is given by

$$\dot{V}_1 = \lambda_i s_i \dot{s}_i, \tag{21}$$

with

$$\lambda_i := \frac{\sigma(s_i)}{\bar{k}_{s_i}^2 - s_i^2} + \frac{1 - \sigma(s_i)}{k_{s_i}^2 - s_i^2}, \tag{22}$$

the derivative of the sliding surface satisfies

$$\dot{s}_i = \dot{z}_{2,i} + \gamma_i \dot{z}_{1,i}. \tag{23}$$

Therefore, the dynamics of the sliding surface becomes

$$\dot{s}_i = f_i(x) + g_i(x_{1,i})u_i + \sum_{j=1, j \neq i}^n g_{i,j}(x_1)u_j + \psi_i(x_1, t) - \dot{y}_{r,i} + \gamma_i z_{1,i}, \tag{24}$$

taking the upper-bound of ψ_i and f_i , and the control action as in (8), one has,

$$\dot{s}_i \leq \|f_i\|^2 + (u_{a_i} + u_{b_i}) + \sum_{j=1, j \neq i}^n g_{i,j}(x_1) + \|\Psi_i\|^2 - \dot{y}_{r,i} + \gamma_i z_{2,i}. \tag{25}$$

Based on Assumptions 1–3 and Equation (16), the derivative of the sliding surface is bounded asymmetrically. Taking the upper and lower bounds for function f_i in Assumption 2 and Equation (3) and selecting the control gains u_{a_i} and u_{b_i} as in (8), Equation (25) becomes

$$\dot{s}_i \leq -\bar{k}_i(t)\text{sign}(s_i) + \|\Psi_i\|^2. \tag{26}$$

Substituting Equation (26) in (23), one has

$$\dot{V}_i \leq \lambda_i s_i \left(-\bar{k}_i(t) \text{sign}(s_i) + \psi_{0,i}^+ + \psi_{1,i}^+ \|x_i\|^2 \right) \tag{27}$$

with the definition of λ as in (22), Equation (27) is equivalent to

$$\dot{V}_i \leq -\frac{\sigma(t)\eta_{b,i}}{\bar{k}_{s_i}(1-\eta_{b,i}^2)} (\bar{k}_i(t)\text{sign}(s_i) + \psi_i^+) - \frac{(1-\sigma(t))\eta_{a,i}}{\underline{k}_{s_i}(1-\eta_{a,i}^2)} (\bar{k}_i(t)\text{sign}(s_i) + \psi_i^-), \tag{28}$$

where $\psi_i^+ = \psi_{0,i}^+ + \psi_{1,i}^+(x^+)^2$ and $\psi_i^- = \psi_{0,i}^- + \psi_{1,i}^-(x^-)^2$. Using the following expressions

$$\text{sign}(s_i) = \frac{s_i}{|s_i|}, \quad |s_i| \leq |\eta_a| |\underline{k}_{s_i}|, \quad |s_i| \leq |\eta_b| |\bar{k}_{s_i}|,$$

Equation (28) turns into

$$\begin{aligned} \dot{V}_i \leq & \frac{\sigma(s_i)}{\bar{k}_{s_i}(1-\eta_{b,i}^2)} \left(\frac{-\bar{k}_i(t)\eta_{b,i}(1-\eta_{b,i})s_i}{\bar{k}_{s_i}\eta_{b,i}} + |\eta_{b,i}|\Psi_i^+ \right) + \\ & \frac{1-\sigma(s_i)}{\underline{k}_{s_i}(1-\eta_{a,i}^2)} \left(\frac{-\bar{k}_i(t)\eta_{a,i}(1-\eta_{a,i})s_i}{|\underline{k}_{s_i}|\eta_{a,i}} + |\eta_{a,i}|\Psi_i^- \right), \end{aligned} \tag{29}$$

Selecting the control gain $k(t)$ as in Equations (13) and (29) becomes

$$\dot{V}_i \leq -\sigma(s_i) \frac{\eta_{b,i}^2}{1-\eta_{b,i}^2} \frac{0.5^{3/2}\mu_i}{\eta_{b,i}} - (1-\sigma(s_i)) \frac{\eta_{a,i}^2}{1-\eta_{a,i}^2} \frac{0.5^{3/2}\mu_i}{\eta_{a,i}}$$

with the application of Lemma 1 part b, the next inequality is valid

$$\dot{V}_i \leq -\frac{\sigma(s_i)}{2} \log\left(\frac{1}{1-\eta_{b,i}^2}\right) \frac{0.5^{1/2}\mu_i}{\eta_{b,i}} - \frac{(1-\sigma(s_i))}{2} \log\left(\frac{1}{1-\eta_{a,i}^2}\right) \frac{0.5^{1/2}\mu_i}{\eta_{a,i}}. \tag{30}$$

Taking into account the result showed in Lemma 2, last equation can be bounded as

$$\begin{aligned} \dot{V}_i \leq & -\sigma(s_i) \frac{1}{2} \log\left(\frac{1}{1-\eta_{b,i}^2}\right) \frac{0.5^{1/2}\mu_i}{\sqrt{\frac{1}{2} \log\left(\frac{1}{1-\eta_{b,i}^2}\right)}} - \\ & (1-\sigma(s_i)) \frac{1}{2} \log\left(\frac{1}{1-\eta_{a,i}^2}\right) \frac{0.5^{1/2}\mu_i}{\sqrt{\frac{1}{2} \log\left(\frac{1}{1-\eta_{a,i}^2}\right)}}, \end{aligned} \tag{31}$$

which is equivalent to

$$\dot{V}_i \leq -0.5^{1/2}\mu_i \left(\sigma(s_i) \sqrt{\frac{1}{2} \log\left(\frac{1}{1-\eta_{b,i}^2}\right)} + (1-\sigma(s_i)) \sqrt{\frac{1}{2} \log\left(\frac{1}{1-\eta_{a,i}^2}\right)} \right). \tag{32}$$

Applying the inequality $\sqrt{a+b} \leq \sqrt{a} + \sqrt{b}$, one finally obtains

$$\dot{V}_i \leq -0.5^{1/2}\mu_i \sqrt{\left(\sigma(s_i) \frac{1}{2} \log\left(\frac{1}{1-\eta_{b,i}^2}\right) + (1-\sigma(s_i)) \frac{1}{2} \log\left(\frac{1}{1-\eta_{a,i}^2}\right) \right)}. \tag{33}$$

Taking the definition of the BLF, Equation (33) is equivalent to next inequality

$$\dot{V}_i \leq -0.5^{1/2} \mu_i V_i^{1/2}. \tag{34}$$

Therefore, the time derivative of $V(s)$ is equivalent to

$$\dot{V}(s) \leq -0.5^{1/2} \sum_{i=1}^n \mu_i V_i^{1/2} \leq -0.5^{1/2} \bar{\mu} V^{1/2} \tag{35}$$

Equation (35) implies the finite-time convergence of the sliding surface with a reaching time defined in Equation (17) in the main theorem [33]. This concludes the proof. \square

6. Numerical Simulations

Orthosis Specifications

Figure 1 describes the robotic orthosis that is made up of three principal sections: (1) the head support that holds the head of the patient preventing falling and (2) the collar structure which supports the whole mechanism. This structure should be positioned on the shoulders of the patient to prevent any cervical damage. Finally, (3) the mechanical actuators that forces the movement of the orthosis.

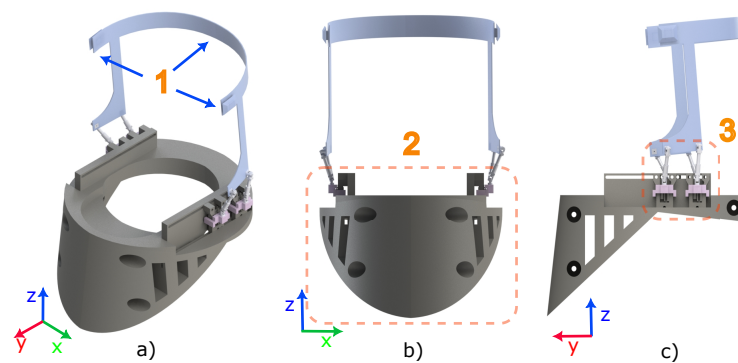


Figure 1. Orthosis design in a CAD software. (a) Isometric view; (b) frontal view; and (c) lateral view.

The movement of actuators allows to control the range, and the trajectory of the neck during rehabilitation therapies. The corresponding motion trajectories should be suggested by professional physicians. Figure 2 shows the class of actuators selected for the orthosis. The orthosis employs linear actuators that generates a movement in the x-y direction.

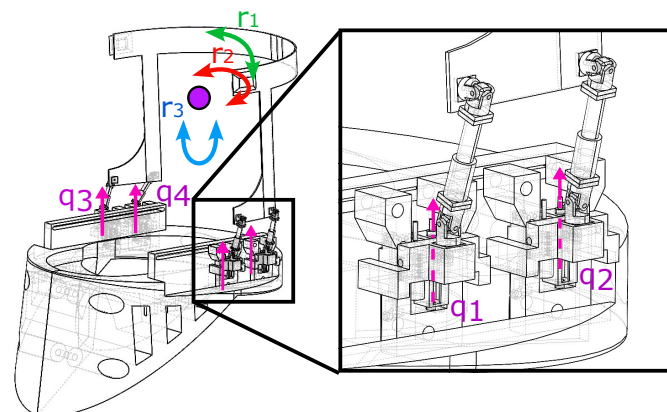


Figure 2. The mechanism of movement generated by a set of linear actuators. The closer view describes the position and orientation of the actuators.

Once the proposal design was approved, the CAD design is exported to Simulink in Matlab to prove the orthosis in a virtual environment. The SimMechanics environment allows to prove virtually the functions of the orthosis. With the measurements of position and velocity obtained from SimMechanics, it is possible to evaluate the control performance for a future implementation. The control must satisfy the neck motion for the rehabilitation according to the trajectories suggested by physicians.

A comparison is done employing a classical PID controller. The control gains employed in this controller are $k_P = 10$, $k_D = 2.5$ and $k_I = 0.5$. For the FOSM controller the gains are $\gamma = 0.002$, $\mu_i = 0.1$. The positive restriction in position is 5.795×10^{-4} m, while the negative restrictions is -5.725×10^{-4} m, the restrictions in velocity were 1 cm/s and -1.3 cm/s. Figure 3 shows the results obtained with the proposed asymmetric FOSM controller. Notice that the position of the orthosis follows the desired trajectories without violating the state restrictions. A comparison against a classical proportional–integral–derivative (PID) controller demonstrates the advantages using the analysis based on BLF. Even though, the results obtained with the PID strategy do not violates the asymmetric state restrictions imposed on the orthosis, the trajectories do not reach the desired ones. Figure 4 describes the tracking trajectory task for the velocity. Similar to previous results the trajectories remain inside the constraints. The initial overshoot presented by the PID controller does not fulfill the state restrictions, while the overshoot provided by the asymmetric FOSM that is smaller than the PID remains inside the restrictions. Notice that the convergence is improved applying the controller proposed in this manuscript. Figure 5 describes the control signal obtained with each approach. Finally, Figure 6 shows the comparison of the tracking error obtained with the PID and the AFOSM. The tracking error resulted from applying the PID is bigger than the one obtained with the AFOSM. These numerical simulations corroborate the theoretical results showed in Theorem 1.

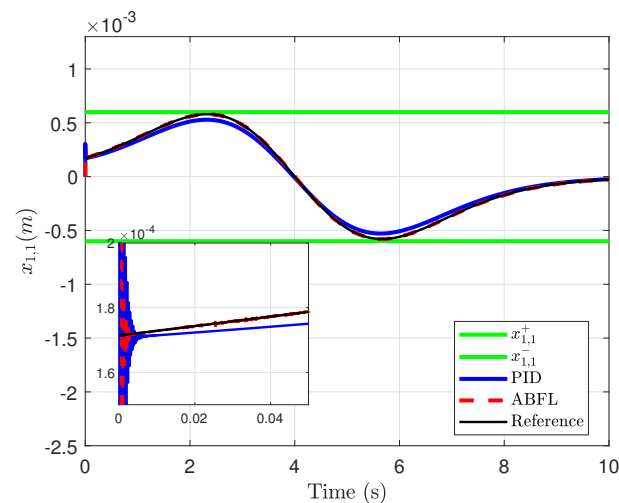


Figure 3. Tracking trajectory of position.

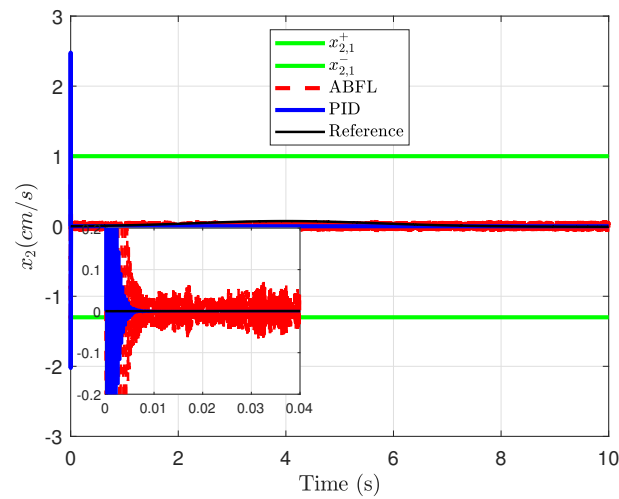


Figure 4. Tracking trajectory of velocity.

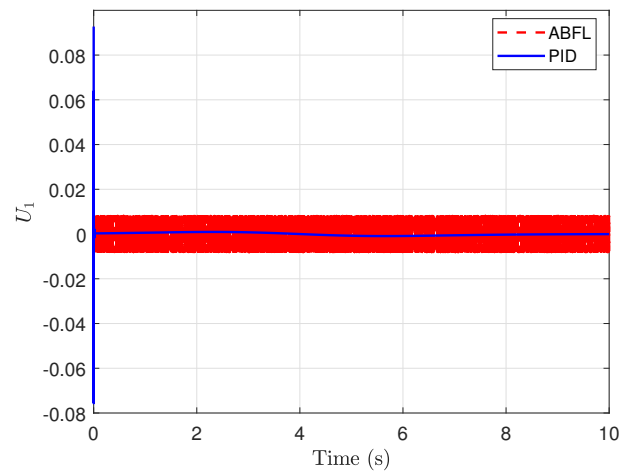


Figure 5. Control signal.

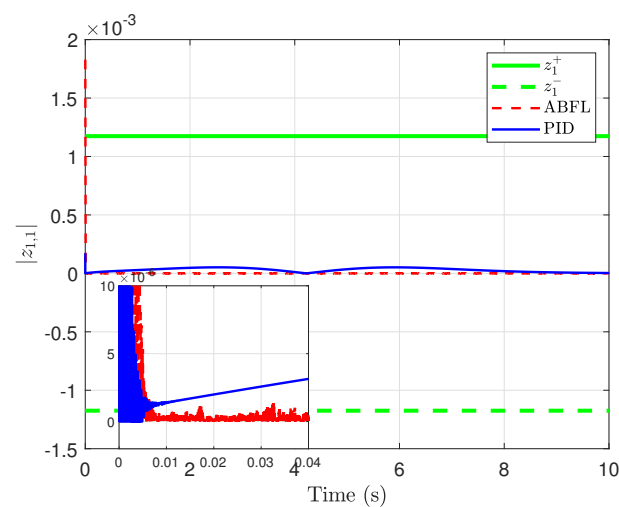


Figure 6. Tracking error for the position.

7. Conclusions

This manuscript showed the control of an orthotic cervical device assuming asymmetric state restrictions based on FOSM and ABLF. The stability analysis demonstrated

the finite-time convergence of the nonlinear system towards the sliding surface and consequently, asymptotic convergence of the tracking error. Numerical results compared the trajectories obtained with classical controllers showing how the trajectories do not fulfil the restrictions when a PID is applied. Further research should be oriented to study time-varying restrictions based on sliding mode approaches and to validate through a clinical study the advantages of using these active devices.

Author Contributions: The work described in this article is the collaborative development of all authors. Methodology and experiments simulation, C.M. and A.L.; writing—original draft preparation and conceptualization, D.C.-O.; Methodology, writing—review and editing, and project administration, M.B. and I.S. All authors have read and agreed to the published version of the manuscript.

Funding: This research was funded by Instituto Politécnico Nacional grant numbers SIP-20221150, SIP-20220916, SIP-20221506, SIP-20226963, SIP-20221746.

Conflicts of Interest: The authors declare no conflict of interest.

Abbreviations

The following abbreviations are used in this manuscript:

BLF	Barrier Lyapunov function
ABLF	Asymmetric Barrier Lyapunov function
SM	Sliding modes
FOSM	First order sliding modes

References

- Bonato, P. Advances in Wearable Technology and Applications in Physical Medicine and Rehabilitation. *J. Neuroeng. Rehabil.* **2005**, *2*, 1–4. [CrossRef] [PubMed]
- Onose, G.; Morcov, M.V.; Sporea, C.; Mirea, A.; Ciobanu, V. Augmentation and Rehabilitation with Active Orthotic Devices. In *Modern Approaches to Augmentation of Brain Function*; Springer: Cham, Switzerland, 2021; pp. 521–548. [CrossRef]
- Gavin, T.; Carandang, G.; Havey, R.; Flanagan, P.; Ghanayem, A.; Patwardhan, A. Biomechanical analysis of cervical orthoses in flexion and extension: A comparison of cervical collars and cervical thoracic orthoses. *J. Rehabil. Res. Dev.* **2003**, *40*, 527–537. [CrossRef] [PubMed]
- Kalita, B.; Narayan, J.; Dwivedy, S.K. Development of active lower limb robotic-based orthosis and exoskeleton devices: A systematic review. *Int. J. Soc. Robot.* **2021**, *13*, 775–793. [CrossRef]
- Ter Wengel, P.V.; de Witt Hamer, P.C.; Pauptit, J.C.; van der Gaag, N.A.; Oner, F.C.; Vandertop, W.P. Early surgical decompression improves neurological outcome after complete traumatic cervical spinal cord injury: A meta-analysis. *J. Neurotrauma* **2019**, *36*, 835–844. [CrossRef] [PubMed]
- Yozbatiran, N.; Francisco, G.E. Robot-assisted therapy for the upper limb after cervical spinal cord injury. *Phys. Med. Rehabil. Clin.* **2019**, *30*, 367–384. [CrossRef] [PubMed]
- Lendraitienė, E.; Smilgiene, L.; Petrusėviciene, D.; Savickas, R. Changes and Associations between Cervical Range of Motion, Pain, Temporomandibular Joint Range of Motion and Quality of Life in Individuals with Migraine Applying Physiotherapy: A Pilot Study. *Medicina* **2021**, *57*, 630. [CrossRef] [PubMed]
- Bell, K.M.; Frazier, E.; Shively, C.; Hartman, R.A.; Ulibarri, J.C.; Lee, J.Y.; Kang, J.D.; Donaldson, W.F. Assessing range of motion to evaluate the adverse effects of ill-fitting cervical orthoses. *Spine J. Off. J. N. Am. Spine Soc.* **2009**, *9*, 225–231. [CrossRef]
- Frigo, C.; Pavan, E. Prosthetic and Orthotic Devices. *Assist. Technol. Concepts Methodol. Tools Appl.* **2013**, 549–613. [CrossRef]
- Karimi, M.T.; Kamali, M.; Fatoye, F. Evaluation of the efficiency of cervical orthoses on cervical fracture: A review of literature. *J. Craniovertebral Junction Spine* **2016**, *7*, 13. [CrossRef]
- Johnson, R.M.; Hart, D.L.; Owen, J.R.; Lerner, E.; Chapin, W.; Zeleznik, R. The yale cervical orthosis: An evaluation of its effectiveness in restricting cervical motion in normal subjects and a comparison with other cervical orthoses. *Phys. Ther.* **1978**, *58*, 865–871. [CrossRef] [PubMed]
- Sarma, J.; Sahai, N.; Bhatia, D. Recent advances on ankle foot orthosis for gait rehabilitation: A review. *Int. J. Biomed. Eng. Technol.* **2020**, *33*, 159–173. [CrossRef]
- Lochner, S.; Huissoon, J.; Bedi, S. Parametric Design of Custom Foot Orthotic Model. *Comput.-Aided Des. Appl.* **2013**, *9*, 1–11. [CrossRef]
- White, A. Some Comments on Cervical Orthoses. In *Clinical Prosthetics and Orthotics*; 2022. Available online: http://www.oandplibrary.org/cpo/pdf/1983_03_005.pdf (accessed on 26 August 2022).
- Kumar, R.; Prakash, A. Efficacy of cervical orthoses in improving neck control of growing children with cerebral palsy: A narrative review. *J. Indira Gandhi Inst. Med Sci.* **2021**, *7*, 90. [CrossRef]

16. Ricotta, V.; Campbell, R.; Ingrassia, T.; Nigrelli, V. A new design approach for customised medical devices realized by additive manufacturing. *Int. J. Interact. Des. Manuf. (IJIDeM)* **2020**, *14*, 1–8. [[CrossRef](#)]
17. Iradi, I.; Zulueta, E.; Teso-Fz-Betoño, D.; Saenz-Aguirre, A.; Fernandez-Gamiz, U. Modeling of Motorized Orthosis Control. *Appl. Sci.* **2019**, *9*, 2453. [[CrossRef](#)]
18. Zhang, H.; Chang, B.; Andrews, J.; Mitsumoto, H.; Agrawal, S. A robotic neck brace to characterize head-neck motion and muscle electromyography in subjects with amyotrophic lateral sclerosis. *Ann. Clin. Transl. Neurol.* **2019**, *6*, 1671–1680. [[CrossRef](#)] [[PubMed](#)]
19. Font-Llagunes, J.; Pàmies-Vilà, R.; Alonso, J.; LUGRÍS, U. Simulation and design of an active orthosis for an incomplete spinal cord injured subject. *Procedia IUTAM* **2011**, *2*, 68–81. [[CrossRef](#)]
20. Chang, B.C.; Zhang, H.; Trigili, E.; Agrawal, S.K. Bio-Inspired Gaze-Driven Robotic Neck Brace. In Proceedings of the 2020 8th IEEE RAS/EMBS International Conference for Biomedical Robotics and Biomechanics (BioRob), New York, NY, USA, 29 November–1 December 2020; pp. 545–550. [[CrossRef](#)]
21. Guzman-Victoria, I.; Salgado, I.; Mera, M.; Chairez, I.; Ahmed, H. Impedance Adaptive Controller for a Prototype of a Whiplash Syndrome Rehabilitation Device. *Math. Probl. Eng.* **2019**, *2019*, 1–21. [[CrossRef](#)]
22. Zhang, H.; Santamaria, V.; Agrawal, S. Applying Force Perturbations Using a Wearable Robotic Neck Brace. In Proceedings of the 2020 IEEE/RISJ International Conference on Intelligent Robots and Systems (IROS), Las Vegas, NV, USA, 25–29 October 2020; pp. 4197–4202. [[CrossRef](#)]
23. Cruz-Ortiz, D.; Chairez, I.; Poznyak, A. Sliding-Mode Control of Full-State Constraint Nonlinear Systems: A Barrier Lyapunov Function Approach. *IEEE Trans. Syst. Man Cybern. Syst.* **2022**, *52*, 6593–6606. [[CrossRef](#)]
24. Tee, K.P.; Ge, S.S.; Tay, E.H. Barrier Lyapunov functions for the control of output-constrained nonlinear systems. *Automatica* **2009**, *45*, 918–927. [[CrossRef](#)]
25. Mera, M.; Salgado, I.; Chairez, I. Robust observer-based controller design for state constrained uncertain systems: Attractive ellipsoid method. *Int. J. Control* **2020**, *93*, 1397–1407. [[CrossRef](#)]
26. Li, Y.X. Barrier Lyapunov function-based adaptive asymptotic tracking of nonlinear systems with unknown virtual control coefficients. *Automatica* **2020**, *121*, 109181. [[CrossRef](#)]
27. Salgado, I.; Mera, M.; Chairez, I. Suboptimal adaptive control of dynamic systems with state constraints based on barrier Lyapunov functions. *IET Control Theory Appl.* **2018**, *12*, 1116–1124. [[CrossRef](#)]
28. Yang, G.; Yao, J.; Dong, Z. Neuroadaptive learning algorithm for constrained nonlinear systems with disturbance rejection. *Int. J. Robust Nonlinear Control* **2022**, *32*, 6127–6147. [[CrossRef](#)]
29. Cruz-Ortiz, D.; Chairez, I.; Poznyak, A. Non-singular terminal sliding-mode control for a manipulator robot using a barrier Lyapunov function. *ISA Trans.* **2022**, *121*, 268–283. [[CrossRef](#)]
30. Zhang, H.; Chang, B.C.; Agrawal, S.K. Using a robotic neck brace for movement training of the head-neck. *IEEE Robot. Autom. Lett.* **2019**, *4*, 846–853. [[CrossRef](#)]
31. Lozano, A.; Ballesteros, M.; Cruz-Ortiz, D.; Chairez, I. Active neck orthosis for musculoskeletal cervical disorders rehabilitation using a parallel mini-robotic device. *Control Eng. Pract.* **2022**, *128*, 105312. [[CrossRef](#)]
32. Nocedal, J.; Wright, S.J. *Numerical Optimization*; Springer Series in Operations Research and Financial Engineering; Springer: New York, NY, USA, 2006; pp. 1–663. Available online: <https://link.springer.com/book/10.1007/978-0-387-40065-5> (accessed on 26 August 2022).
33. Polyakov, A.; Fridman, L. Stability notions and Lyapunov functions for sliding mode control systems. *J. Frankl. Inst.* **2014**, *351*, 1831–1865. [[CrossRef](#)]